Impact of Processing Parameters in Plasma Electrolytic Oxidation (PEM) on Corrosion Resistance of Magnesium Alloy Type AZ91

Talal A. Aljohani[1]*, Sami Aljadaan[2], Meteb T. Bin Rubayan[3], Fuad Khoshnaw[4]

[1,2,3] National Centre for Corrosion Technology, King Abdulaziz City for Science and Technology, KACST, Riyadh, Saudi Arabia

[1] taljohani@kacst.edu.sa https://orcid.org/0000-0003-3530-8809

[2] saljadaan@kacst.edu.sa, [3] mbinrubayan@kacst.edu.sa

[4] School of Engineering and Sustainable Development, De Montfort University, Leicester, UK
fuad.hassankhoshnaw@dmu.ac.uk https://orcid.org/0000-0002-4467-1944

Abstract

This study aims to investigate the effect of the processing parameters in plasma electrolytic oxidation (PEO) on the corrosion resistance of magnesium alloy type AZ91. The PEO coatings were prepared on the samples using alkaline-based electrolyte. Both unipolar and bipolar, different frequencies and duty cycles were applied. Corrosion tests, using potentiodynamic polarisation (PDP), linear and cyclic, and electrochemical impedance spectroscopy (EIS) techniques, were applied on the as-received and PEO coated samples. Scanning electron microscopy was used to investigate the surface morphology, e.g. micropores, as well as to measure the thickness of the coated layer with changing the processing parameters. The results show that the size of micropores is interrelated to the duty cycle percentage and current polarities, as the higher frequency causes thinner coating layers, with fewer micropores, consequently higher corrosion resistance. In addition, increasing the duty cycle, a denser and more compact coating was obtained. The XRD results showed a missing peak of the α-Mg phase in a PEO coated sample using Bipolar, the highest frequency (1666 Hz) and the highest duty cycle (66.6%). The mils per year calculations showed that the PEO coated have lower corrosion rate by at least 8 times than the as-received alloy.

1. Introduction

The features such as high strength/weight ratio, good machinability, thermal conductivity, and electromagnetic shielding make the magnesium alloys highly used in different industries such as automobile, aerospace and electronics industries [1–5]. Magnesium alloys, also, are used in clinical applications such as biodegradable implants for cardiovascular, musculoskeletal, and general surgery [6][7]. However, due to its high reactivity, magnesium has low corrosion resistance and the oxide film on its surface easily can break [8]. Therefore, researchers are continuously attempting to improve the performance of magnesium alloys in various fields.

Anodizing, where aluminium is coated on magnesium, is among the traditional methods, which has been used for a while, to improve the corrosion resistance, however, because the mechanical properties of aluminium are relatively low, e.g. yield strength, hence, other attempts have been

conducted, such as adding nanoparticles and forming a hybrid coating, using plasma electrolyte oxidation (PEO) [9–15] [16–18].

PEO electrolytic plasma oxidation (EPO), which is also known as MAO, is an electrochemical surface treatment process for generating oxide coatings on metals. This process is similar to the anodizing, but with applying higher potentials. In general, the process depends on the modification of a conventional anodically grown oxide film through applying an electric field much greater than the dielectric breakdown field of the oxide. Therefore, during discharging, the resulting plasma-chemical reactions contribute to the growth of the coating. Coating properties depend on the substrate alloy, the electrolyte and on the electrical parameters[1–4,19–21].

The mechanism of the PEO coatings on magnesium alloys has been investigated through applying electrochemical measurement, and optical spectroscopy and acoustic emission spectrometer. The performance of the coatings has been characterized by measuring the wear and corrosion rates. Besides, the biocompatibility tests of PEO coatings have been considered [22].

Francis et al [16] studied the pre-treatment of magnesium alloy type AZ91 in alkaline silicate solution by anodic oxidation in the presence of sodium salicylate. The electrochemical corrosion behaviour of anodized films was investigated using electrochemical impedance spectroscopy. The results showed a significant increase in the corrosion resistance. Liang et al [17] worked on two types of PEO coatings on AM50 magnesium alloy using pulsed DC plasma electrolytic oxidation process in an alkaline phosphate and acidic fluozirconate electrolytes.. The corrosion behaviour of the coated samples was evaluated by electrochemical techniques in neutral 0.1 M NaCl solution. The results showed that the PEO coating which was composed of only MgO suffered from localized corrosion, whereas the PEO coating with ZrO2 compounds showed higher stability and provided efficient corrosion protection. Lu et al [18] used PEO with nano-and micro-sized SiO_2 particles to seal the porosity, then tested at different KOH concentrations. Yang et al [23] used PEO to improve the corrosion resistance and biocompatibility of porous MgO-CaP coatings by adding hydroxyapatite (HA) particles. The results showed that most HA particles were reactively incorporated into the PEO coatings and the coating microstructure was significantly modified with increasing the concentration of HA, which resulted in higher corrosion resistance. Hussein et al [24] studied the PEO mechanism through investigating the formation of a coating layer, up to 110 μm thickness on AJ62 Mg alloy. They found that during the PEO process some of the metal cations are transferred outwards from the substrate and react with anions to form ceramic coatings. At the same time, due to the high electric field in the discharge channels, oxygen anions transfer toward the magnesium substrate and react with Mg^{+2} cations to form a ceramic coating. Lu et al [25] studied the influence of SiO_2 particles on the microstructure, phase composition, corrosion and wear performance of PEO coatings on AM50 Mg alloy. Different electrolyte compositions were applied to fabricate coatings in an alkaline, phosphate-based electrolyte, aiming to control the incorporated amount of the particles in the layer. It was found that the uptake of particles was accompanied by the coating growth at the initial stage, while the particle

content remained unchanged at the final stage, which is dissimilar to the evolution of the coating thickness. They found that the corrosion performance of the coating mainly depends on the barrier property of the inner layer, while wear resistance primarily relies on the coating thickness[25,26].

Cao et al [27] studied PEO process with an alkaline borate solution - contained organic additive without F, P, and Cr - on Mg-based alloy type AZ91D alloy using 50 Hz AC anodizing technique, through applying different anodizing parameters. It was found that the formation of the anodic films was always coupled with sparking and oxygen evolution, whose intensity changed with the additive and anodizing voltage. However, the addition of organic additive, to seal the pores, showed no significant effect on corrosion resistance.

Sreekanth et al [26] developed PEO coatings on AZ31 magnesium alloy using alkaline silicate with KOH as a base electrolyte system, adding different sodium aluminate, sodium tetra-borate, potassium titanium fluoride, trisodium ortho-phosphate and urea as additives. The results showed that the sample treated by PEO in the electrolyte solution, containing sodium tetra-borate as an additive, showed higher corrosion resistance.

Ghasemi et al [28] used four different electrolytes including either potassium or sodium hydroxides. Electrolyte conductivity and breakdown voltage were measured to correlate the property of the coating to the type of the electrolyte. The EIS results indicated the presence of porous and compact layers in the structure of the PEO coatings. While the corrosion resistance was mainly attributed to the compact layer, the role of the porous layer, as a barrier, against corrosion was negligible.

Duan et al [29] described the growth process of the oxide film formed on magnesium alloy AZ91D under PEO in an alkaline silicate solution. It was found that at the initial stage (before the occurrence of sparking), the growth rate of PEO films is low, the elements (O, Mg, Al and Si) contents were varied and the donor concentration in the film was kept at a high level. However, after sparking, the PEO films showed a higher growth rate. On the other hand, the results showed that with increasing the treated time, the thickness of PEO films and transfer resistance to ions and electrons were also increased; thereby, the growth rate of the PEO films was decreased.

Due to the complexity of the formation of PEO coatings, there are still some factors requiring in-depth studies. To fill this gap, this research has examined the impact of using unipolar and bipolar currents on PEO coating of AZ91 alloy.

2. Materials and Experimental Works

Magnesium alloy type AZ91 was used in this study, the chemical composition in wt% - as it is provided by NeoCast, is 9.04 Al, 0.695 Zn, 0.28 Mn, 0.0026 Fe, 0.00107 Be, 0.031 Si, 0.0013 Cu, and Mg balance. Samples were cut into rectangular shapes with dimensions equal to 11 x 4.5 x 1 cm. the sample area was fixed as 130cm^2. No pre-treatments were applied to the samples before the plasma electrolytic process. The PEO process was performed in a polyvinyl chloride container (PVC) lined

with a $1m^2$ stainless-steel sheet which was used as a counter electrode, while the specimen was acting as working electrode. The PEO was carried out in an alkaline solution comprising 3g/L of potassium hydroxide [KOH]. The whole system was connected to a cooling system to keep the temperature around 25 C and the solution was kept mixed using air agitation. For safety measures, the whole system was placed inside a fume hood.

To investigate the effect of polarity of the process on the coating layer structure and its thickness, both unipolar and bipolar methods were applied, using different frequency and duty cycles. The experiment duration was 300 sec. Table 1 describes the PEO electrical conditions that were applied. Duty cycle % for working electrode was calculated based on the following equation:

$$\text{duty cycle} = \frac{t\,on}{t\,on + t\,off} \quad (1)$$

were t_{on} is on time, t_{off} is off time, and (t_{on}+ t_{off}) is the whole time

Table 1 The applied parameters; frequencies, currents, and coating thickness

Samples	Polarity	Frequency (Hz)	Off/On (ms)	Duty cycle %	Working electrode (mA)	Counter electrode (mA)	Ave. Coating thickness (μm)
AZ91- PEO 1	Unipolar	1000	0.7/0.3	30	30	0	14
AZ91- PEO 2	Bipolar	1000	0.7/0.3	30	30	10	13
AZ91- PEO 3	Bipolar	1666	0.2/0.4	66.6	30	10	6
AZ91- PEO 4	Bipolar	1000	0.5/0.5	50	30	10	16

3. Electrochemical tests and characterisation

A Potentiostat type Bio-Logic SP-200 and flat corrosion cell - with three electrodes - were used, to perform the electrochemical corrosion tests. The platinum and saturated calomel electrode were used as counter and reference electrodes respectively. The potential scan rate for the polarization technique was 0.166 mVs^{-1} to ensure a steady-state condition. A linear polarization scan was applied in a short potential range of ±25 mV. The EIS tests were performed at the open-circuit potential, $E_{corr,}$ by applying a sinusoidal voltage between ±10 mV within a frequency range of 10 mHz to 100 kHz. The electrochemical measurements were performed at aerated 0.5M sodium chloride at 298 K.

The surface morphology of the corroded samples was investigated using a scanning electron microscope (SEM) type JSM-IT300 InTouchScope™ in combination with an X-MaxN Oxford energy-dispersive X-ray spectroscopy (EDS) analyser. The crystallinity of the structure was explored using X-ray diffraction type JEOL JDX-8030 X-ray diffractometer with Cu Kα radiation operating at 40 kV and 30 mA at a scan rate of 2°/min.

4. Results and discussion

4.1 Surface morphology

Figure 1 shows SEM images of the Mg samples coated by PEO before and after corrosion tests. Figures 2a and 2b show the as-received AZ91 alloy before and after applying the corrosion test respectively. The coated samples showed micro-holes, with different sizes and shapes, which were evolved by applying different frequency and duty cycle %.

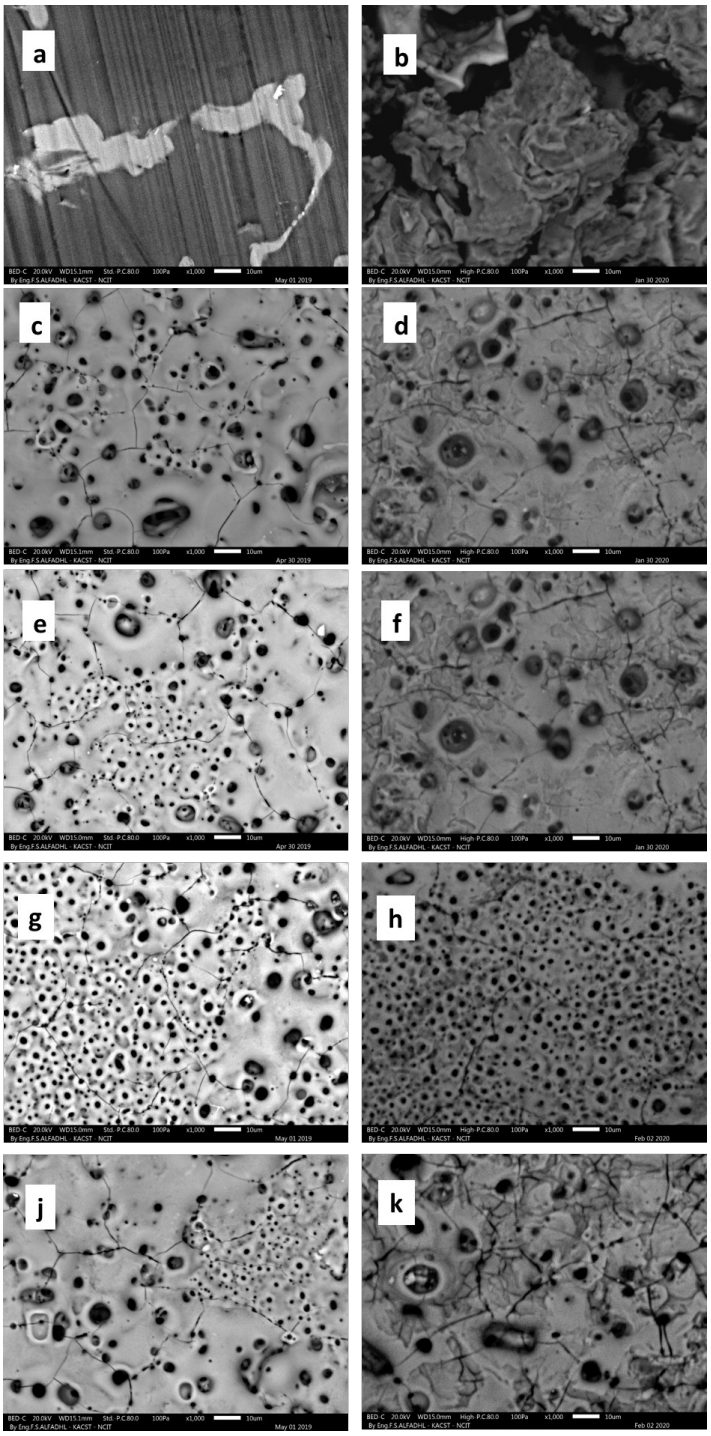

Figure 1: Surface morphologies before (left) and after (right) corrosion test: pure AZ91 (a and b), AZ91- PEO 1 (c and d), AZ91- PEO 2 (e and f), AZ91- PEO 3 (g and h) and AZ91- PEO 4 (j and k).

Figure 1c shows large holes for the coated sample processed with 30 mA, unipolar- PEO 1, while Figure 1g shows that the pores sizes were smaller for the sample prepared with PEO 3 parameters - by reducing the processing time and increasing the frequency. This agrees with Gh. Barati et al [22] results, their study found that pore size is a function of the discharge density and processing time. The

coated samples, as shown in Figures 2 d,f,h,k, however, show no significant corrosion except the surface was slightly darkened.

Figure 2 shows the as received alloy AZ91 after electrochemical corrosion test. It shows a severe corrosion compared to coated samples presented in Figure2 b,d,f,h,k.

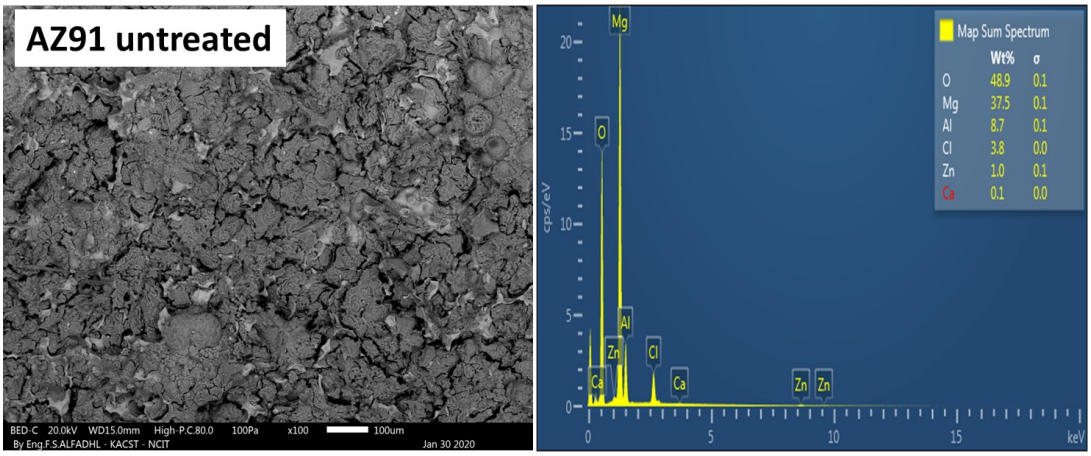

Figure 2 SEM images and EDS analysis of as-received AZ91 after corrosion test examined in aerated 0.5M sodium chloride at 298 K.

Figure 3 shows that the coating thickness for samples prepared at low frequency i.e. 1000 Hz ranges around 14 µm. The thickness significantly decreased by increasing frequency to 1666 Hz, see Table 1, which indicates that both the thickness and pores size are affected by frequency. The images show thicknesses between samples coated under similar frequencies but with different polarities, PEO-1 and 2, moreover between the samples coated under the same frequencies by different high-duty percentages, PEO -2 and 4.

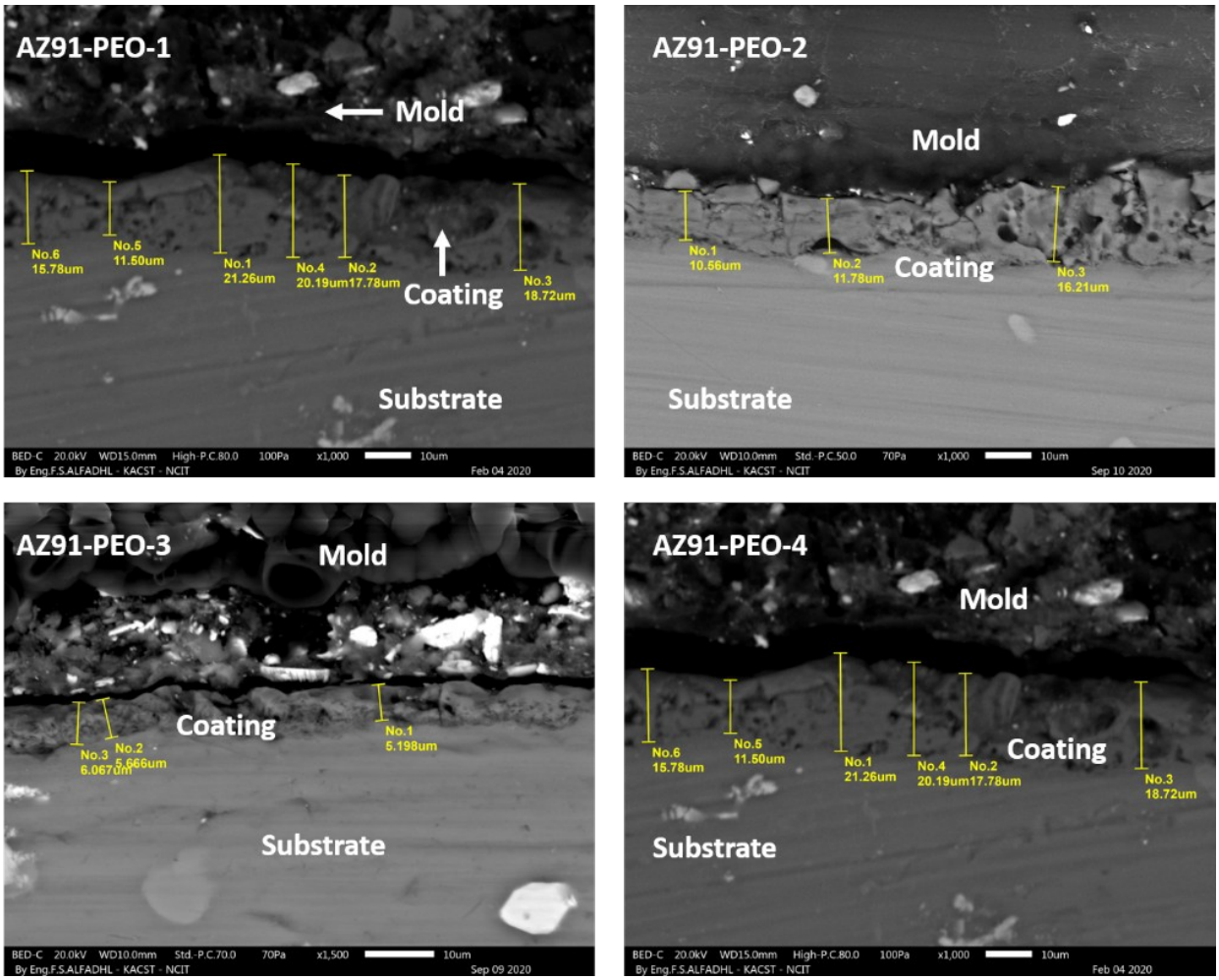

Figure 3 Cross-section images of samples with different PEO coatings parameters.

4.2 Microstructure

Figure 4 shows XRD patterns that refer to the appearance of the related elements. The indices indicate the composition of Mg, MgO, $MgAl_2O_4$ and $Mg_{17}Al_{12}$. The layered result is constituted mainly by Mg and MgO due to the composition of the alloy and the electrolyte while the other elements due to the reflection of the alloy. Comparing the peaks of the PEO sample with the as-received AZ91 sample shows slight changes in the intensity of the compositions that can be attributed to the changes in the coating parameters, for example, lower and higher peaks were for the as-received AZ91 and AZ91-PEO-4, respectively.

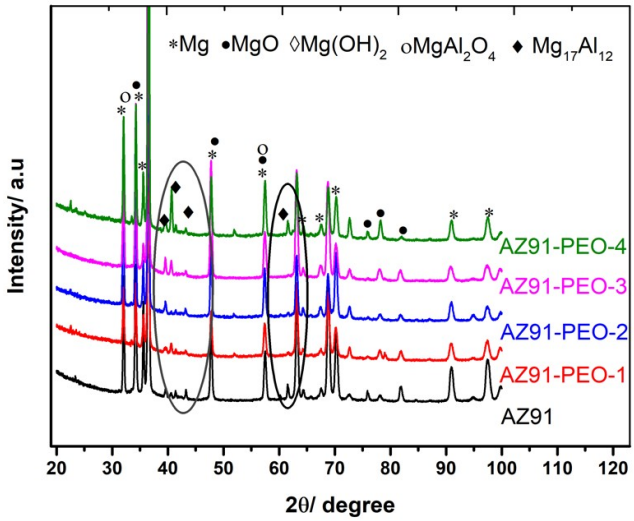

Figure 4: XRD patterns for as-received AZ91 and different PEO coated samples.

Figure 5a shows the XRD patterns of the samples after electrochemical corrosion tests. The peak intensity for as-received AZ91 significantly increased after its exposure to corrosion, while the opposite is true for the PEO coated samples, as the peak intensity decreased. Besides, the as-received AZ91 and all the PEO coated samples, except the AZ91-PEO-3, display an extra peak at = 34.7º which is associated with α-Mg [30]. Figures 2 and 4 showed that the PEO-3 had a distinct surface morphology and thickness with smaller micropores and more compacted coatings.

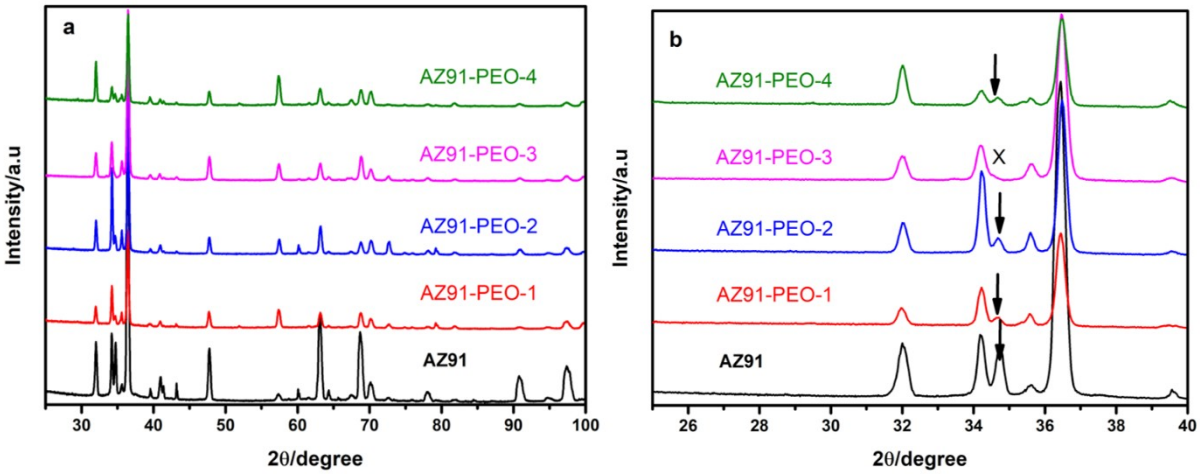

Figure 5: Full spectrum of XRD patterns obtained from as-received AZ91 and PEO coated samples after electrochemical corrosion test examined in aerated 0.5M sodium chloride at 298 K (a), selected region from 26-40 2θ° to show the missing peak.

4.3 Corrosion Measurements

Figure 6 shows the free corrosion potential versus immersion time. All the PEO coatings showed a shift in potential toward the positive potentials, i.e. more passive. Fluctuations in the potentials are appeared which can be attributed to the porosities on the coating surface. The as-received AZ91 sample shows no alternation in potential. The PEO-1 shows the highest peak, the widest range between the lowest and highest peaks, and most frequently peaks, while the PEO 2 and PEO 3 show less oscillation due to their small size pores, see Figure 1.

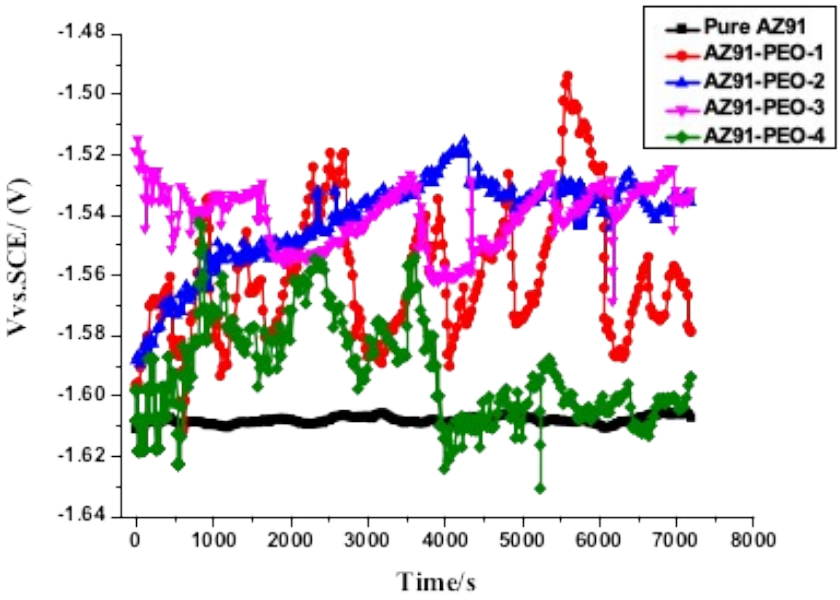

Figure 6: Open circuit potential versus time in the sodium chloride solution [0.5 M].

To investigate the corrosion performance of the coatings at sodium chloride [0.5 M], after reaching a stable free corrosion potential within 2 hours of immersion, the EIS tests were applied on the samples. Figure 7, Nyquist plots, shows only one capacitive semicircle. The increase in its size indicates better corrosion protection of the PEO samples. For the low-frequency PEO sample, an inductive loop was not observed, which is an indication that the PEO process protects the dissolution and localized corrosion of the AZ91 alloy. While the inset part of the figure shows an inductive loop for the as-received alloy. The semicircle behaviour is attributed to the charge transfer process whereas the inductive loop is attributed to the dissolution of the substrate at the coating interface. Similar observations were reported by [11,24,31].

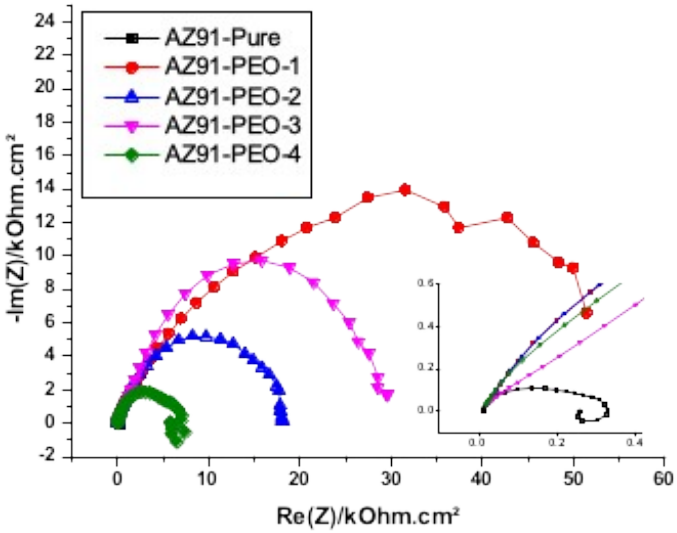

Figure 7: Nyquist plots of PEO coatings performance examined in 0.5 M of sodium chloride. The inset is the zoom-in impedance of the as-received AZ91.

Figure 8a, Bode plots, shows the enhancement of corrosion resistance after PEO treatment. The polarisation resistance extrapolated at low frequency (log f = 0) which was increased from 1 x 10^2 Ω to 1 x 10^4 Ω, indicating a better corrosion performance. Moreover, Figure 8b, shows that the phase angle of PEO coatings, for the high frequency, reached about -60º, indicating that PEO coatings provided better corrosion protection. In particular, the PEO-3 sample showed higher and wider capacitance like performance at intermediate and high frequency. This is attributed to the dense, i.e. less porous, coatings obtained by applying higher pulsing frequency, see Figure 1.

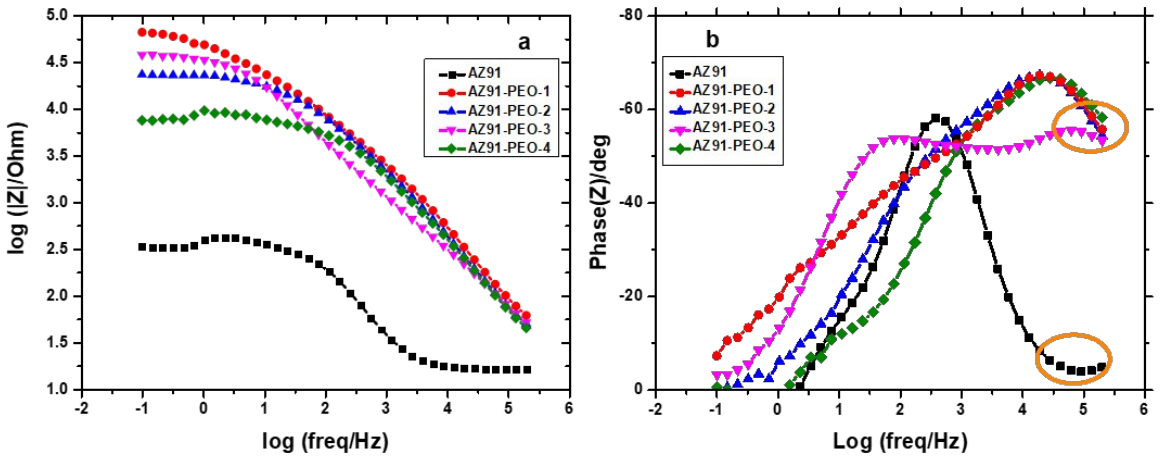

Figure 8 Bode plots (a) log |Z| vs. log (freq/Hz), and (b) phase angle vs. log (freq/Hz) of AZ91 and PEO coatings performance examined in 0.5 M of sodium chloride.

Furthermore, the EIS data were modelled using EC labV10.37 software and the Randomize+ simplex method to examine the corrosion mechanism of the coatings at the electrode/ electrolyte interface. The EIS data were fitted using two equivalent circuit models shown in Figures 9a and 9b for the as-received AZ91 and coated samples respectively. Table 2 lists the fitting results.

Table 2 The EIS fitting results of pure AZ91 alloy and different PEO coatings on AZ91 alloy examined in 0.5 M of sodium chloride. Two equivalent circuits were used.

Samples	R_s ($\Omega.cm^2$)	CPE1 (Ω^{-1} . s^n . cm^{-2})	n_1	R_p ($\Omega.cm^2$)	CPE2 (Ω^{-1} . s^n . cm^{-2})	n_2	R_{ct} ($\Omega.cm^2$)	R_L($\Omega.cm^2$)	L (H. cm^{-2})
AZ91	12.54	2.22×10^{-5}	0.86	NA	NA	NA	299	1135	481
AZ91- PEO-1	15.4	2.33×10^{-7}	0.83	1909	5.25×10^{-6}	0.48	6097	NA	NA
AZ91- PEO-2	12.49	3.80×10^{-7}	0.81	3125	2.19×10^{-6}	0.60	15510	NA	NA
AZ91- PEO-3	6.06	1.89×10^{-6}	0.68	1375	1.02×10^{-6}	0.74	29423	NA	NA
AZ91- PEO-4	4.9	6.69×10^{-6}	0.75	5484	7.17×10^{-6}	1	1320	NA	NA

The equivalent circuit model, for the as-received sample, displays five elements i.e. R_s, CPE1, R_{ct}, R_L, and L for solution resistance, charge transfer resistance, constant phase element, pitting resistance, and inductance respectively. The sample showed small charge resistance and a short time constant of about 150 s. On the other hand, the EC model for the PEO coated samples, has no inductance and pitting corrosion resistance. The EC for PEO coatings displays two constant phase elements, CPE1and CPE2, and two resistances, which are R_p and R_{ct}, in addition to the solution resistance (R_s). At high frequency, a capacitive semicircle is dominated by CPE1 and polarization resistance (R_p) which are related to the outer layer of the PEO coatings. At low frequency, CPE2 and charge transfer resistance (R_{ct}) are depicting the inner layer of the PEO coatings. A similar observation was obtained by Cue et al. [31] and Ling et al. [17].

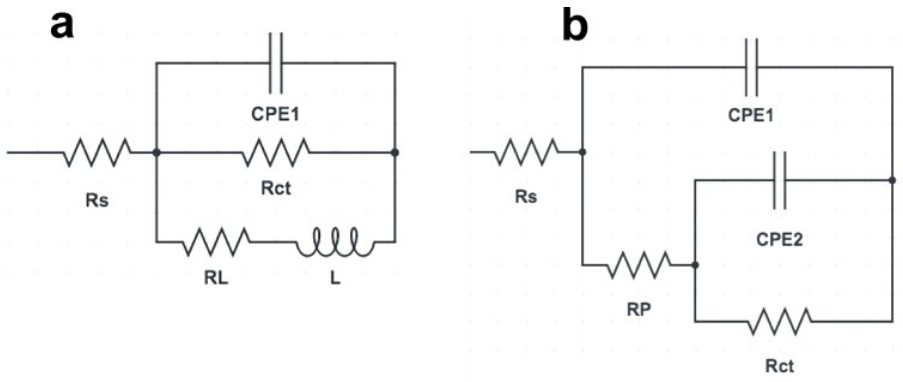

Figure 9: The equivalent circuits model for, a: as-received AZ91, b: PEO coated alloys.

Figure 10 shows potentiodynamic polarization curves, which indicate a considerable improvement in the corrosion resistance of PEO coated samples. The current density of the PEO coated samples decrease by two orders of magnitudes. Also, the PEO samples show a passive range at high oxidative potentials. Table 3 shows the extrapolation results of the potentiodynamic curves, see Figure 10. Table 3 shows that the corrosion current density of the as-received alloy decreased from 60 μAcm^{-2} to around 1.7 μAcm^{-2} for the PEO samples. While the corrosion potentials of the as-received and PEO alloys were similar. The PEO-3 showed a wide range of passivation which complies with the results shown in Bode plots, also see Figure 8b.

Table 3 Corrosion properties obtained from potentiodynamic polarisation curves.

Samples	βa ($mV.dec^{-1}$)	-βc ($mV.dec^{-1}$)	E_{corr} (V/SCE)	I_{corr} (μAcm^{-2})	mmpy
AZ91	23.3	198	-1.479	60.5	1.642
AZ91-PEO-1	85.7	215	-1.424	0.739	0.023
AZ91- PEO 2	96.6	106	-1.495	1.02	0.027
AZ91- PEO 3	141	116	-1.514	2.2	0.060
AZ91- PEO 4	284	253	-1.510	1.744	0.047

Corrosion resistances were extracted through applying linear polarization resistance (LPR) from a slope of the linear current-potential dependence at the free corrosion potential following Stern and Geary equation 2[32]:

$$i_{corr} = \frac{1}{2.3} \frac{b_a b_c}{b_a + b_c} \left(\frac{di}{dE} \right)_{E_{corr}} = \frac{B}{R_p} \quad (2)$$

Where B, icorr, Rp are Tafel constant, corrosion current and polarization resistance respectively.

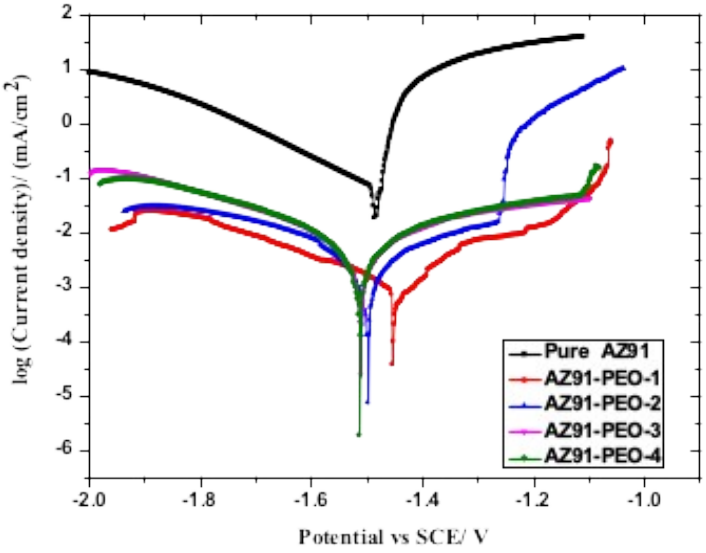

Figure 10: Potentiodynamic polarization curves of PEO coated samples carried out in 0.5 M sodium chloride.

Figure 11 compares the results obtained by cyclic potentiodynamic curves with both the potentiodynamic polarization and EIS results. The results show that current densities decreased for PEO coated samples. However, all PEO coated and the as-received AZ91 samples show positive hysteresis and negative re-passivation potential E_{rep}. This indicates that electrolytes were diffused into the micropores and instigated localized corrosion after a long time of immersion.

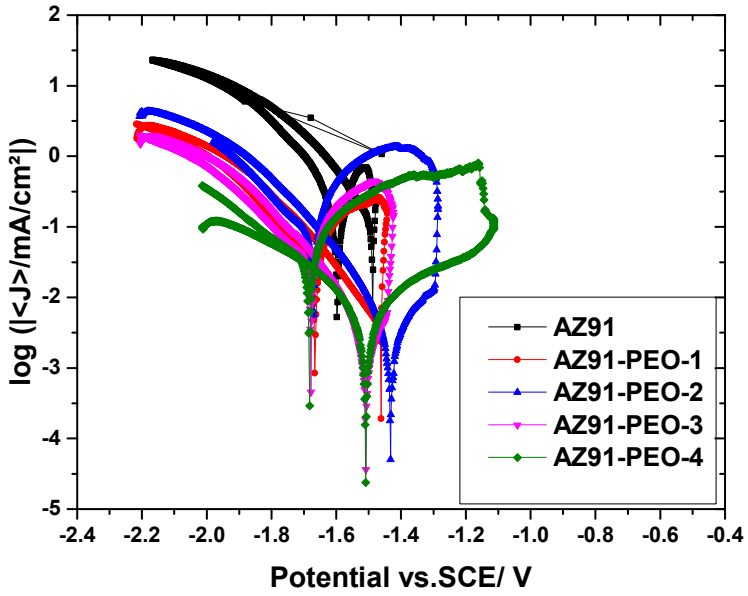

Figure 11: Cyclic potentiodynamic polarization curves of coated AZ91 alloys in 0.5 M of NaCl solution.

Table 4 Corrosion properties obtained from linear polarization resistance (LPR) curves.

Samples	βa ($mV.dec^{-1}$)	-βc ($mV.dec^{-1}$)	Ecorr (V/SCE)	Rp Ohm. Cm^2	R2	Icorr (μAcm^{-2})	mmpy
AZ91	23.3	198	-1.602	247	0.994	36.763	0.993
AZ91-PEO-1	85.7	215	-1.568	40238	0.994	0.662	0.017
AZ91-PEO 2	96.6	106	-1.535	18135	0.997	1.212	0.032
AZ91-PEO 3	141	116	-1.600	5861	0.994	4.720	0.127
AZ91-PEO 4	284	253	-1.584	8042	0.991	7.234	0.195

Table 4 shows the outcomes of the above tests and finding out the corrosion rate in mils per year (mmpy). The results show that all the PEO coated samples have lower corrosion rate compared with the as-received AZ91 alloy. The highest mmpy value for the PEO samples is still lower than the as-received by at least 8 times.

5. Conclusions

- PEO coating improves the corrosion resistance of magnesium alloy type AZ91.
- Bipolar current PEO processing mode with high frequency provides smaller microprobe than unipolar.
- Bipolar waveform with higher frequencies provides a thinner, but denser, coating layer, consequently higher corrosion resistance.
- The AZ91-PEO3 displayed , smaller micropores, extended plateau (capacitor like behaviour) over middle and high frequency ranges.
- The mmpy values showed a large ratio, around 8:1, between the as-received to the PEO coated samples.

Acknowledgment

The authors are grateful to King Abdulaziz City for Science and Technology (KACST) in the Kingdom of Saudi Arabia for supporting this project (Ref. no. 37502500) and for De Montfort University in the United Kingdom for scientific and technical supports.

Conflict of interest

The authors declare no potential conflict of interest.

Talal A. Aljohani: Conceptualization; corrosion analysis; project administration; supervision; writing−original draft. **Sami Aljadaan:** validation; plotting data; support; **Meteb T. Bin Rubayan:** Project administration; validation; support; **Fuad Khoshnaw:** investigation; methodology; writing and editing.

References

1. Kaseem, M.; Hussain, T.; Rehman, Z.U.; Ko, Y.G. Stabilization of AZ31 Mg alloy in sea water via dual incorporation of MgO and WO3 during micro-arc oxidation. *J. Alloys Compd.* **2021**, *853*, 157036, doi:10.1016/j.jallcom.2020.157036.

2. Bordbar-Khiabani, A.; Yarmand, B.; Mozafari, M. Effect of ZnO pore-sealing layer on anti-corrosion and in-vitro bioactivity behavior of plasma electrolytic oxidized AZ91 magnesium alloy. *Mater. Lett.* **2020**, *258*, 126779, doi:10.1016/j.matlet.2019.126779.

3. Heydarian, A.; Atapour, M.; Hakimizad, A.; Raeissi, K. The effects of anodic amplitude and waveform of applied voltage on characterization and corrosion performance of the coatings grown by plasma electrolytic oxidation on AZ91 Mg alloy from an aluminate bath. *Surf.*

Coatings Technol. **2020**, *383*, 125235, doi:10.1016/j.surfcoat.2019.125235.

4. Mena-Morcillo, E.; Veleva, L. Degradation of AZ31 and AZ91 magnesium alloys in different physiological media: Effect of surface layer stability on electrochemical behaviour. *J. Magnes. Alloy.* **2020**, *8*, 667–675, doi:10.1016/j.jma.2020.02.014.

5. Mordike, B.L.; Ebert, T. Magnesium Properties — applications — potential. **2001**, *302*, 37–45.

6. Witte, F.; Abeln, I.; Switzer, E.; Kaese, V.; Meyer-Lindenberg, A.; Windhagen, H. Evaluation of the skin sensitizing potential of biodegradable magnesium alloys. *J. Biomed. Mater. Res. - Part A* **2008**, *86*, 1041–1047, doi:10.1002/jbm.a.31713.

7. Witte, F. The history of biodegradable magnesium implants: A review. *Acta Biomater.* 2010, *6*, 1680–1692.

8. Pourbaix, M.; Zhang, H.; Pourbaix, A. Presentation of an Atlas of chemical and electrochemical equilibria in the presence of a gaseous phase. *Mater. Sci. Forum* **1997**, *251–254*, 143–148, doi:10.4028/www.scientific.net/msf.251-254.143.

9. Zhao, L.; Cui, C.; Wang, Q.; Bu, S. Growth characteristics and corrosion resistance of micro-arc oxidation coating on pure magnesium for biomedical applications. *Corros. Sci.* **2010**, *52*, 2228–2234, doi:10.1016/j.corsci.2010.03.008.

10. Song, Y.; Dong, K.; Shan, D.; Han, E.H. Investigation of a novel self-sealing pore micro-arc oxidation film on AM60 magnesium alloy. *J. Magnes. Alloy.* **2013**, *1*, 82–87, doi:10.1016/j.jma.2013.02.009.

11. Dong, K.; Song, Y.; Shan, D.; Han, E.H. Corrosion behavior of a self-sealing pore micro-arc oxidation film on AM60 magnesium alloy. *Corros. Sci.* **2015**, *100*, 275–283, doi:10.1016/j.corsci.2015.08.004.

12. Mathis, A.; Rocca, E.; Veys-Renaux, D.; Tardelli, J. Electrochemical behaviour of titanium in KOH at high potential. *Electrochim. Acta* **2016**, *202*, 253–261, doi:10.1016/j.electacta.2015.11.027.

13. Zhang, X.P.; Zhao, Z.P.; Wu, F.M.; Wang, Y.L.; Wu, J. Corrosion and wear resistance of AZ91D magnesium alloy with and without microarc oxidation coating in Hank's solution. *J. Mater. Sci.* **2007**, *42*, 8523–8528, doi:10.1007/s10853-007-1738-z.

14. Cui, L.Y.; Fang, X.H.; Cao, W.; Zeng, R.C.; Li, S.Q.; Chen, X.B.; Zou, Y.H.; Guan, S.K.; Han, E.H. In vitro corrosion resistance of a layer-by-layer assembled DNA coating on

magnesium alloy. *Appl. Surf. Sci.* **2018**, *457*, 49–58, doi:10.1016/j.apsusc.2018.06.240.

15. Karpushenkov, S.A.; Shchukin, G.L.; Belanovich, A.L.; Savenko, V.P.; Kulak, A.I. Plasma electrolytic ceramic-like aluminum oxide coatings on iron. *J. Appl. Electrochem.* **2010**, *40*, 365–374, doi:10.1007/s10800-009-0005-1.

16. Francis, A.; Virtanen, S.; Turhan, M.C.; Boccaccini, A.R. Investigating the effect of salicylate salt in enhancing the corrosion resistance of AZ91 magnesium alloy for biomedical applications. *BioNanoMaterials* **2015**, *2015*, doi:10.1515/bnm-2015-0008.

17. Liang, J.; Srinivasan, P.B.; Blawert, C.; Dietzel, W. Comparison of electrochemical corrosion behaviour of MgO and ZrO2 coatings on AM50 magnesium alloy formed by plasma electrolytic oxidation. *Corros. Sci.* **2009**, *51*, 2483–2492, doi:10.1016/j.corsci.2009.06.034.

18. Lu, X.; Blawert, C.; Zheludkevich, M.L.; Kainer, K.U. Insights into plasma electrolytic oxidation treatment with particle addition. *Corros. Sci.* **2015**, *101*, 201–207, doi:10.1016/j.corsci.2015.09.016.

19. Yerokhin, A.L.; Nie, X.; Leyland, A.; Matthews, A.; Dowey, S.J. *Plasma electrolysis for surface engineering*; 1999; Vol. 122;.

20. Zheng Yin, Renhua He, Yang Chen, Zhou Yin, Kun Yan, Kun Wang, Hong Yan, Honggun Song, Chengxin Yin, Hongyu Guan, Chao Luo, Zhi Hu, Chassagne Luc, Effects of surface micro–galvanic corrosion and corrosive film on the corrosion resistance of AZ91–xNd alloys.| Applied Surface Science, 2021;Vol.536,147761. https://doi.org/10.1016/j.apsusc.2020.147761.

21. Rakoch, A.G.; Monakhova, E.P.; Khabibullina, Z. V.; Serdechnova, M.; Blawert, C.; Zheludkevich, M.L.; Gladkova, A.A. Plasma electrolytic oxidation of AZ31 and AZ91 magnesium alloys: Comparison of coatings formation mechanism. *J. Magnes. Alloy.* **2020**, *8*, 587–600, doi:10.1016/j.jma.2020.06.002.

22. Barati Darband, G.; Aliofkhazraei, M.; Hamghalam, P.; Valizade, N. Plasma electrolytic oxidation of magnesium and its alloys: Mechanism, properties and applications. *J. Magnes. Alloy.* 2017, *5*, 74–132.

23. Yang, J.; Lu, X.; Blawert, C.; Di, S.; Zheludkevich, M.L. Microstructure and corrosion behavior of Ca/P coatings prepared on magnesium by plasma electrolytic oxidation. *Surf. Coatings Technol.* **2017**, *319*, 359–369, doi:10.1016/j.surfcoat.2017.04.001.

24. Hussein, R.O.; Northwood, D.O.; Nie, X. The effect of processing parameters and substrate composition on the corrosion resistance of plasma electrolytic oxidation (PEO) coated

magnesium alloys. *Surf. Coatings Technol.* **2013**, *237*, 357–368, doi:10.1016/j.surfcoat.2013.09.021.

25. Lu, X.; Chen, Y.; Blawert, C.; Li, Y.; Zhang, T.; Wang, F.; Kainer, K.U.; Zheludkevich, M. Influence of SiO2 particles on the corrosion and wear resistance of plasma electrolytic oxidation-coated AM50 Mg alloy. *Coatings* **2018**, *8*, doi:10.3390/COATINGS8090306.

26. Sreekanth, D.; Rameshbabu, N.; Venkateswarlu, K. Effect of various additives on morphology and corrosion behavior of ceramic coatings developed on AZ31 magnesium alloy by plasma electrolytic oxidation. *Ceram. Int.* **2012**, *38*, 4607–4615, doi:10.1016/j.ceramint.2012.02.040.

27. Cao, F.H.; Cao, J.L.; Zhang, Z.; Zhang, J.Q.; Cao, C.N. Plasma electrolytic oxidation of AZ91D magnesium alloy with different additives and its corrosion behavior. *Mater. Corros.* **2007**, *58*, 696–703, doi:10.1002/maco.200704050.

28. Ghasemi, A.; Raja, V.S.; Blawert, C.; Dietzel, W.; Kainer, K.U. Study of the structure and corrosion behavior of PEO coatings on AM50 magnesium alloy by electrochemical impedance spectroscopy. *Surf. Coatings Technol.* **2008**, *202*, 3513–3518, doi:10.1016/j.surfcoat.2007.12.033.

29. Duan, H.; Yan, C.; Wang, F. Growth process of plasma electrolytic oxidation films formed on magnesium alloy AZ91D in silicate solution. *Electrochim. Acta* **2007**, *52*, 5002–5009, doi:10.1016/j.electacta.2007.02.021.

30. Esmaily, M.; Mortazavi, N.; Svensson, J.E.; Halvarsson, M.; Blücher, D.B.; Jarfors, A.E.W.; Wessén, M.; Johansson, L.G. Atmospheric Corrosion of Mg Alloy AZ91D Fabricated by a Semi-Solid Casting Technique: The Influence of Microstructure. *J. Electrochem. Soc.* **2015**, *162*, C311–C321, doi:10.1149/2.0341507jes.

31. Cui, L.Y.; Gao, S.D.; Li, P.P.; Zeng, R.C.; Zhang, F.; Li, S.Q.; Han, E.H. Corrosion resistance of a self-healing micro-arc oxidation/polymethyltrimethoxysilane composite coating on magnesium alloy AZ31. *Corros. Sci.* **2017**, *118*, 84–95, doi:10.1016/j.corsci.2017.01.025.

32. Stern, M. Electrochemical Polarization. *J. Electrochem. Soc.* **1957**, *104*, 559, doi:10.1149/1.2428653.